Alignment and Deformation of the Cryostat in the CADS Injector Ⅱ

Jiandong Yuan*, Lizhen Ma, Yuan He, Bin Zhang, Juihui Zhang,Guozhen Sun

（Institute of Modern Physics，Chinese Academy of Sciences，509#, Nanchang Road, Lanzhou, GanSu, China, 730000）

15th International Workshops on Accelerator Alignment, FERMI, Batavia,USA 8-12 October,2018

Abstract: Thermal contraction and expansion of the Cryostat will affect its reliability and stability. To optimize and upgrade the Cryostat, we analyzed the heat transfer in a cryo-vacuum environment from the theoretical point first. The simulation of cryo-vacuum deformation based on a finite element method was implemented respectively. The completed measurement based on a Laser Tracker and a Micro Alignment Telescope was conducted to verify its correctness. The monitored deformations were consistent with the simulated ones. After the predictable deformations in vertical direction have been compensated, the superconducting solenoids and Half Wave Resonator cavities approached the ideal “zero” position under liquid helium conditions. These guaranteed the success of 25 MeV@170 uA continuous wave protons of Chinese accelerator driven subcritical system Injector Ⅱ. By correlating the vacuum and cryo-deformation, we have demonstrated that the complete deformation was the superposition effect of the atmospheric pressure, gravity and thermal stress during both the process of cooling down and warming up. The results will benefit to an optimization for future Cryostat’s design.

Keywords: Cryostat; Deformation; Laser tracker; Micro alignment telescope; Superconducting solenoid; Half wave resonator cavity

1 Introduction

A well designed Cryostat can easily reduce power consumption and the length of an accelerator, and allow the accelerator to be run continuously. It is becoming increasingly important in the superconducting linac [1].The Cryostat is the challenge for the alignment of a superconducting linear accelerator owing to the invisibility and the ultra-low temperature characteristics (4 K). The Institute of Modern Physics in Chinese Academy of Sciences is developing an accelerator driven subcritical system (CADS) Injector Ⅱ [2]. The CADS will accelerate protons with a beam current of 10 mA to about 1.5 GeV to produce neutrons for the transmutation of nuclear waste [3]. To avoid generating any beam orbit distortion, the magnet magnetic center must be on the beam axis, so the deformation of cold components has challenging requirements [4]. From the theoretical point, there are generally three approaches to deal with the deformation on the working condition [5]. One is to maintain the alignment upon the cool down. In this approach, the structure is designed so that the cool down is absolutely symmetric. The other is to allow realignment once cold. In this approach, components must be realigned after they reached their final cryogenic temperature. As we all know the above two situations cannot easily be reached.

The final approach is to allow the components to change in a predictable and repeated way. There are currently four different methods to measure this objective. The European organization for nuclear research developed a double-sided Brandeis CCD Angle Monitor (BCAM) [6]. The Japanese high-energy accelerator research organization adopted white light interferometer (WLI) [7]. The German Electron Synchrotron [8], Institute of High Energy Physics of the Chinese Academy of Sciences [9] and Fermi National Accelerator Laboratory [10] employed a Wire Position Monitor (WPM) to monitor the contraction. The French national large heavy-ion accelerator adopted a micro-alignment telescope to align Cryostat intuitively [11]. However, these above methods only investigated the cryo-deformation, did not consider the effect of the negative pressure of the vacuum. Ref [12] has estimated the pressure distribution inside the cavity string

*Supported by National Natural Science Foundation of China (Study on the online monitoring of cryomodule (NO：11605262))

Corresponding author: Jiandong Yuan; E-mail: yuanjiandong@impcas.ac.cn

using a mathematical model. Ref [13] analyzed the deformation induced by temperature differences, but did not correlate the cryo-vacuum deformation.

However, the exact deformation mechanism of cryostat under cryo-vacuum condition remains unclear so far. Therefore, we investigate the correlation of the cryo-vacuum deformation of the cryostat in CADS Injector Ⅱ. The paper is organized as follows. In section 2 we provide a brief description of the requirements on the cryostat; then we analyze the heat transfer under vacuum cryo-environments in section 3. We provide the simulated results in section 4, and the monitored results in section 5, respectively. Then we exam and discuss the results between the measured with the simulated ones in section 6. Finally we draw conclusions; the cryo-deformation is closely related to vacuum condition and the structure of the cryostat. The deep investigation will benefit for the optimization [14] and upgrade [15][16] of Cryostat design for the China Initiative Accelerator Driven Subcritical system (CiADS).

2 Design Requirements of the Cryostat

The CADS injector Ⅱ project includes four cryostats. As shown in the Fig. 1, each cryostat houses two posts (G10), two titanium frames, one helium vessel, six Half Wave Resonator (HWR) cavities, five superconducting (SC) solenoids, one copper thermal shield and five beam position monitors (BPM), etc. The vacuum chamber of each Cryostat is a rectangular box of dimension 4.2 m × 1.5 m × 1.6 m. The HWR cavity, SC solenoid, and other cold mass were fixed on two titanium frames. And the titanium frame was hung on the top plate of the vacuum chamber. The SC HWR cavity is selected owing to its high accelerating gradient. The SC solenoid is chosen to offer superior transverse focusing gradient with shorter length compared with quadrupole at low energy section. The low-beta HWR cavities with $\beta = 0.10$ and $\beta = 0.15$ in 162.5 MHz and spoke cavities with $\beta = 0.21$ in 325 MHz were chosen to accelerate the beam from the 2.1 MeV at the RFQ to 25 MeV. The designed operating temperature is 4.4-4.5 K by bath cooling. Their alignment will be carried out at room temperature first, and then the predictable compensation will be implemented. The allowable deformation of the cold mass at 77 K is 1 and 3 mm in the horizontal and vertical direction, respectively [17].

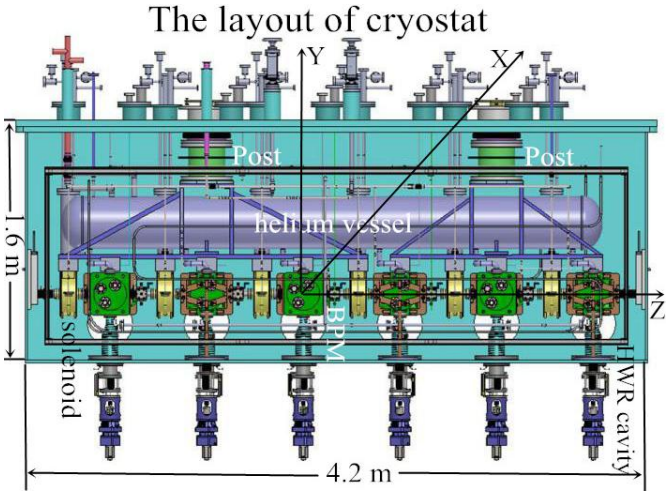

Fig. 1 The Layout of Cryostat (Color online)

Some principles should be implemented when designing a cryostat. The first is to define and prioritize the requirements such as operating temperatures, heat load and safety from the start of the project. Then only use materials shown to be appropriate for cryogenic temperatures, take advantage of existing codes and standards if possible and use tested commercial solutions whenever possible [5]. Cryostat design also includes system integration of complex devices that have to be housed inside the insulation vacuum and often at cryogenic temperatures: such as Beam Position Monitors (BPM), cryogenic instrumentation (temperature, pressure, level, and mass flow sensors) and control devices (valves, servo-motors, and mechanical transmissions), electrical circuits for magnets' and cavities' powering and protection, etc. [16].

3 Heat Transfer Principles

Generally, heat transfer includes the sum of thermal radiation, convection, and sometimes conduction transfer. Usually, more than one of these processes occurs in a given situation. Since the Cryostats are operated in a cryo-vacuum

environment, there is no convective heat transfer in the static heat loads [17][18]. There are only thermal radiation [19] from the "hotter" environment and direct thermal conduction through the cold mass supports, power couplers and the feedthroughs [20]. Thermal conduction is the transfer of heat by microscopic diffusion of particles or quasi-particles within a body due to a temperature gradient [21]. In many cases, the analysis may be simplified by the use of thermal conductivity integrals. In this approach, the conduction heat transfer in one dimension is given by [22] (Equation 1): where A_i and L_i are the cross-sectional area of conducting surface (in m^2) and length of conducting surface (in m) through which the conduction heat flows in each component and k_i is the thermal conductivity of the corresponding material.

$$Q_{Conduction} = \sum_{i=1}^{n} \frac{A_\perp}{L_i} \int_{77K}^{295K} k_i dT \quad (1)$$

Thermal radiation is an electromagnetic radiation generated by the thermal motion of charged particles. In general, the most of the elements in accelerator cryostats are approximate to opaque, meaning that all energy is either absorbed or reflected. Assuming $A_2/\ \varepsilon_2$ is the area/effective emissivity of the vacuum vessel and A_1/ε_1 is area/effective emissivity of the internal thermal shield, σ is the Stefan-Boltzmann constant, and T_2 and T_1 are the temperature of the vacuum vessel and thermal shield, respectively ($T_2>T_1$). While for the cryostat with parallel flat plates (A), the surfaces of the vacuum vessel and thermal shield ($A_2 \approx A_1=A$) were placed together at a close distance, the approximate heat radiation can be derived from the heat exchange balance is given by the Equation 2:

$$Q_{Radiation} = \sigma \cdot A \cdot (T_2^4 - T_1^4) \Big/ \left(\frac{1}{\varepsilon_1} + \frac{1}{\varepsilon_2} - 1\right) \quad (2)$$

According to Equation 2, reducing radiation heat loads can be obtained by reducing the size of the vacuum vessel A_2, as well as reducing both ε1 and ε2 (in particular ε1, which has the largest effect) . During the cool-down, the thermal shield receives radiative heat flux from both the external vacuum vessel and from the internal cold mass. To sum up, multi-layer insulation (MLI) and low emissivity materials (aluminum, copper or Ni plating) for the thermal shield are both effective methods to reducing the heat radiation [16].

4 Simulations

A finite element method (FEM) was used to analyze the cryo-vacuum stress and deformation. The finite method is an approximate Ritz method combined with a variational principle applied to continuum mechanics. The plate is discretized into a finite number of elements, connected at their nodes and along hypothetic inter-element boundaries. FEM utilizes an indirect, iterative approach to converge to a solution of the systems of equations. The procedure begins with an initial "guess" for a solution. With each subsequent iteration, a better approximation result (assuming that each successive approximation satisfies the established criteria for convergence) and convergence to a solution is attained after a finite number of iterations [23]. Solid Works was used to modeling first; and then the cryostat model was imported in ANSYS, meshed with four surfaces unit; finally the cryo-vacuum deformation was simulated and monitored.

4.1 Vacuum deformation

A high-vacuum level must be achieved [12] to guarantee an effective cool-down process and operations for the Cryostat. However the unbalanced gravity load and vacuum negative pressure will results in the deformation of the vacuum chamber. Hence the thorough stress and strain analysis of the vacuum chamber under atmospheric pressure and self-gravity should be carried out. The vacuum chamber is made of 316 L stainless steel and its strength will weaken under cryo-vacuum conditions. Therefore there must have some stiffeners (100×150 mm) on the vacuum chamber. The thickness of the stiffeners' wall is 8 mm made of 316 L stainless steel. The thickness of the top cover plate, side plate and base plate is 30, 25, and 30 mm, respectively. As shown in Tab. 1, the boundary conditions and loads in the model are as following: Given that 1.5 tons of gravity was exerted on the two insulating supports, one atmospheric pressure (0.1MPa) was applied to the six surfaces of the vacuum chamber; the four bottom supports were fixed.

Table. 1 The boundary conditions, loads and their acting position of the vacuum deformation

NO	Boundary Conditions and Loads	Acting Position

1	The four bottom supports were fixed	Four bottom supports
2	Integral Gravity (1.5 tons, 750 kg per post)	The center of the two posts (G10)
3	Atmospheric Pressure (101.3 KPa)	The six external surface of the vacuum chamber

As shown in Fig. 2, the equivalent stress (peak stress value is 183 MPa appears in the two reinforcing bars of the connected stiffeners) of the main vacuum vessel without organic glass is lower than the allowable stress of the corresponding materials (198 MPa of 316 L stainless steel). The max stress (205.9 MPa) is located at the position of the organic glass.

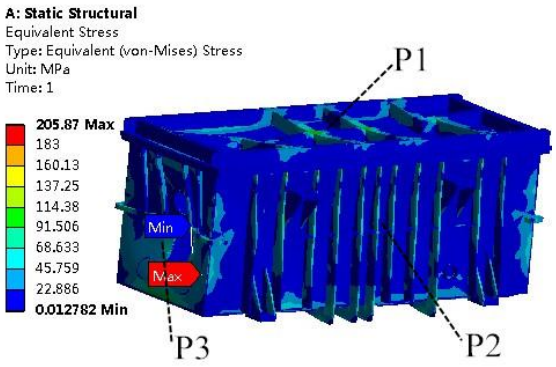

Fig. 2 Stress Simulation (Color online)

As seen from Fig. 3, based on the coordinate frame shown in Fig. 1, the vacuum deformation occurs mainly in the central area around the horizontal vertical and longitudinal zone of vacuum chamber were 0.53, 1.24 and 1.06 mm, respectively. Furthermore the central region is larger than the lateral area. In the horizontal and longitudinal direction, the deformation of the side plate presents an obvious symmetry and equivalence. While in the vertical direction, the max deformation (1.24 mm) occurs in the bottom of the vacuum chamber on account of the lacking of the reinforced stiffeners. However, the max deformation of the top cover plate (1.06 mm) appears mainly in the center of the two posts.

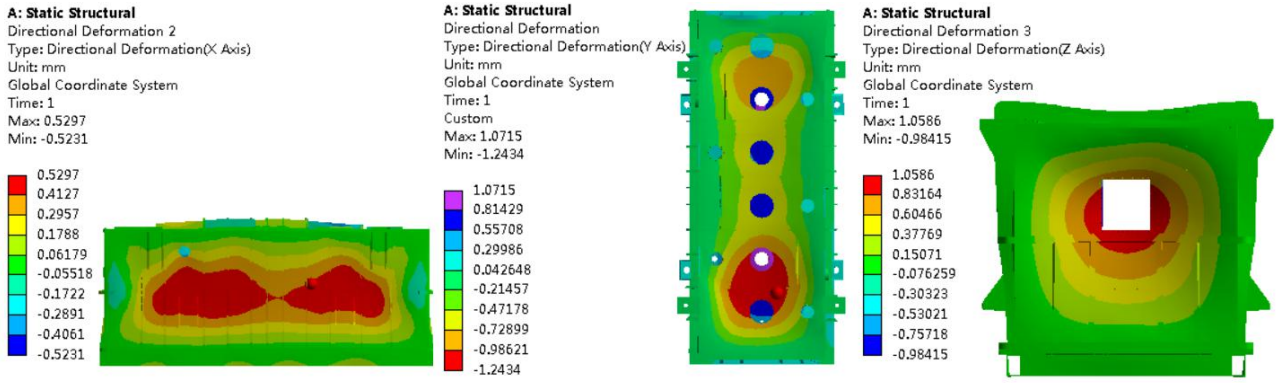

(a) Horizontal (b) Vertical (c) Longitudinal

Fig. 3 Vacuum Simulation (Color online)

4.2 Cryo-deformation

The two cooling experiments were conducted using liquid nitrogen. According to the analysis of a statically determinate structure induced by temperature changes [24][25], the cryo-deformation is proportional to the coefficient of thermal expansion, temperature change and length, if the temperature of the member is decreased uniformly throughout its length.

In the model, the SC magnets, helium tank, and its welding bracket used 316 L stainless steel material. The suspended support used titanium material. The HWR cavity horizontally positioned was made of pure niobium and immersed in a liquid helium vessel made of titanium (TA2). The copper coupler was vertically positioned and to be cooled by cold helium gas. Its tuner made of Ti alloy was put at one side of the cavity. The contact surface of support was operated at 300 K. The thermal conductivity of materials varies strongly with a temperature between 300 and 77 K.

The surface heat load of 77 K (316 L stainless steel) was 0.9 W/m^2 [26][27]. As shown in Tab. 2, the boundary conditions and load [28] contain a self-gravity of the cold mass assembly, a distributive load of temperature, a force of the cold mass assemblies and the top suspending rods.

Table. 2 The boundary conditions, loads and their acting position of the cryo-deformation

NO	Boundary Conditions and Loads	Acting Position
1	The four rods were fixed	Four top suspending rods
2	Integral Self-Gravity (1.5 tons, 750 kg per post)	The center of the two posts (G10)
3	Cold mass Temperature (4K)	The center of the cold mass
4	Rods Temperature (295K)	Four top suspending rods

As shown in the Fig. 4, single cavity was employed to simulate the temperature distribution and cryo-deformation in order to simplify the calculation. The thermal and mechanical analysis used same mesh. The SC solenoid, HWR cavity and helium vessel were the cooling source on the normal operation process. The temperature of the titanium frame is 7-9 K, which was cooling through the conducted heat from the above cooling source.

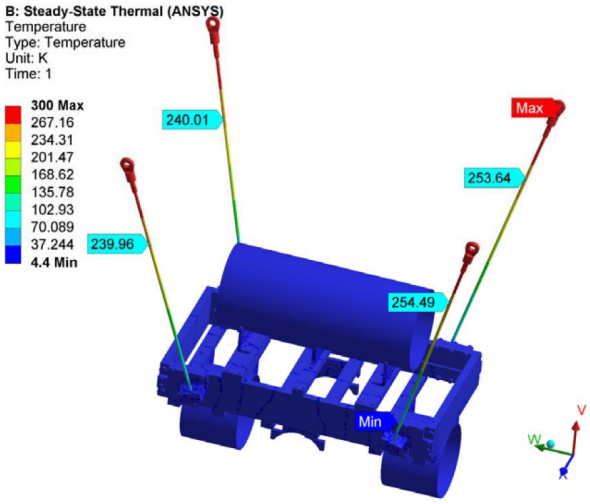

Fig. 4 Temperature Simulation (Color online)

As shown in Fig. 5, according to the mechanical characteristics of cold mass [29], the simulated results of the solenoid and HWR cavity were contracted 0.77 mm in the horizontal and raised 2.98 mm in the vertical direction, respectively. The position changing of the cold mass was in the controlling range of design requirements. In the horizontal direction, the deformation of the solenoid and HWR cavity presents an obvious symmetry and equivalence. While in the vertical direction, the max deformation (2.98 mm) occurs in the bottom of the solenoid and HWR cavity on account of the absence the fixed bolts.

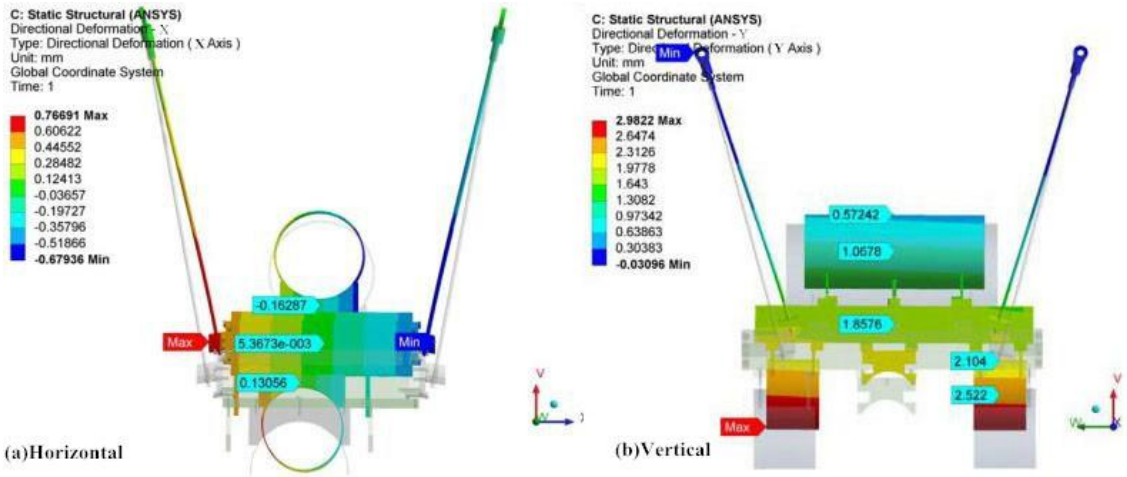

Fig. 5 Cryo-Simulation (Color online)

5 Monitoring

5.1 Vacuum deformation

In order to verify the correctness of the vacuum simulation, we have monitored the horizontal, vertical, longitudinal deformation using a Laser Tracker at the position of p2, p1, p3 of Fig. 2. As Seen in Fig. 6, the four operations of vacuum pump started at 11:10 on December 1, 20:58 on December 1, 21:43 on December 5 and 7:37 on December 6, 2016, respectively. The vacuum level reached 0.1 Pa about 3 hours later and 10^{-3} Pa about 11 hours later. The four procedures of vacuum release started at 16:55 on December 1, 17:13 on December 2, 4:01 on December 6 and 3:52 on December 7, 2016, respectively. The vacuum level returned to 0.1 Pa about 8 hours later. The Laser Tracker system is able to compensate for temperature and humidity effects based on the measurement conditions. The monitored vacuum deformations are central 0.66 mm in the horizontal direction, 1.32 mm in vertical direction and 0.89 mm in longitudinal direction resulting from the balanced vacuum pressure as an effect of evacuation, respectively (with respect to the initial zero position). The monitored deformations are consistent with the simulated ones: the differences are 0.13 mm in the horizontal direction, 0.08 mm in the vertical direction and 0.17 mm in the vertical direction compared with Fig. 3, respectively.

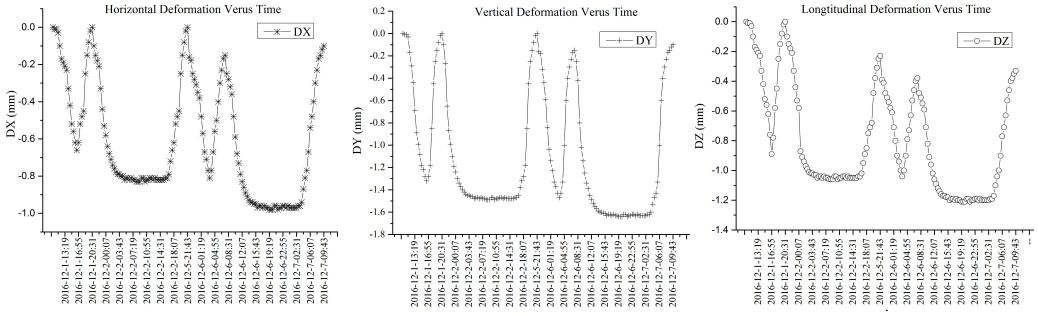

Fig. 6 vacuum deformation (DX: horizontal; DY: vertical; DZ: longitudinal)

5.2 Cryo-deformation

We have investigated the mechanism of vacuum deformation of the chamber. Next, we examined the effect of the expansion with heat and contraction with cold on the cold mass inside of the vacuum chamber. The Micro Alignment Telescope (MAT) was adopted to monitor the deformation at the position of the inside of the vacuum chamber. As shown in Fig. 7, the monitored cryo-deformation versus temperature shows close agreement with the simulated ones (in Fig. 5) during two thermal cycling without compensation. Since the target was located on the right (below) of solenoid and HWR cavity, a plus sign means that it is close to center(rise up)； A minus sign means that it is off center (go down). Noted that the data in Fig. 7 was taken after the vacuum pumped (cooled down) and released (warmed up). After being cooled down 24 hours, the cold mass was contracted 0.8 mm in horizontal and 2.87 mm in vertical direction on average, respectively (with respect to the pumped ones). And then cold mass has warmed up to 290 K after warmed up 24 hours, and has expanded 0.5 mm horizontal and 1 mm vertical on average, respectively(with respect to the released ones). The differences between simulated and monitored were 0.03 mm in horizontal and 0.11 mm in vertical direction on average, respectively.

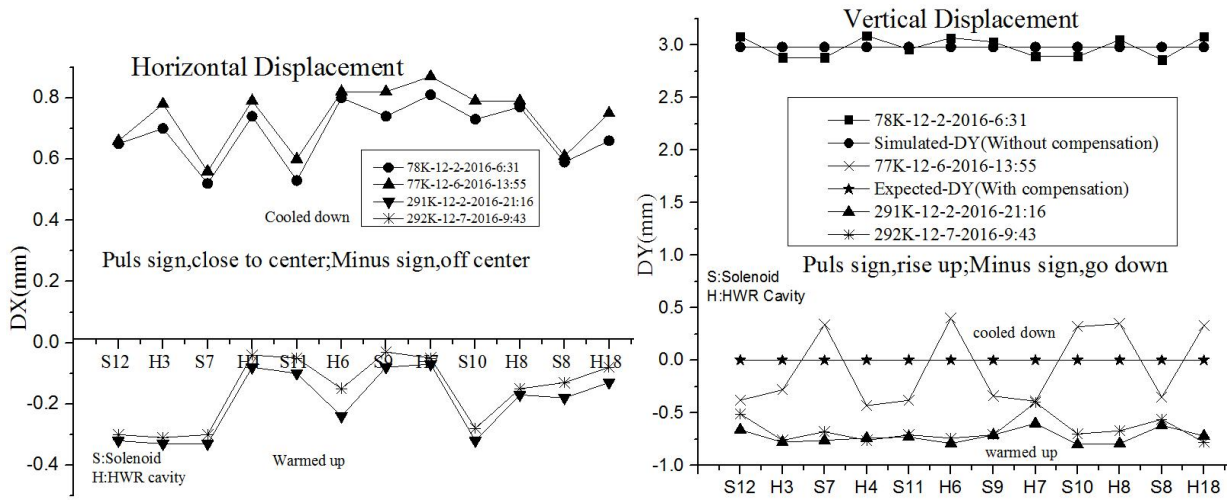

Fig. 7 Cryo-deformation

6 Discussions

Though Fig. 6 suggests that most of the vacuum deformation belong to elastic deformation, there is also a little plastic deformation during the pumping process. Furthermore, we have noticed that the difference of temperature exerted a subtle influence on the vacuum chamber, which demonstrated that the vacuum chamber was not sensitive to thermal deformation. In addition to the continuous monitoring, the discrete monitoring at the position of cavity and solenoid inside of the vacuum chamber were also furnished by the MAT. Our previous research [29] has shown that the direction of the movement of the cold mass on the vacuum condition seems different from each other in the horizontal direction resulting from the unbalanced vacuum pressure during the pumping process. However, the directions of the movement of the cold mass on the vacuum condition seem to coincide with each other in the vertical direction and were all central. This was close agreement with the results of ref [9] and ref [30]. Fig. 6 also showed the cryo-deformation of the vacuum chamber, the results indicate that temperature field seems exert a little influence on the chamber because of the isolated G10 support resulting from its low thermal conductivity.

Table. 3 Results Comparison between simulating and monitoring

Deformation		Simulated	Monitored	Differences
Vacuum	DX (mm)	0.53	0.66	0.13
	DY (mm)	1.24	1.32	0.08
	DZ (mm)	1.06	0.89	0.17
Low temperature	DX (mm)	0.77	0.8	0.03
	DY (mm)	2.98	2.87	0.11

The precise predictable compensation is essential for the normal operation of the continuous wave beam. The influences of vacuum under different structure on the cryo-deformation are different in the vertical direction. Due to the supports were located on the inside surface of the top or bottom vacuum chamber, the direct vertical stress exerted on the inside cold mass (cavity, solenoid and so on) comprised the negative atmospheric pressure (the force normal to the surface per area), gravity and thermal stress during the process of cooling down. Therefore, the complete deformations in the vertical direction were the superposition effect of the above stresses. However, the horizontal deformation resulted only from the thermal stress. As shown in Tab. 3, since the negative atmospheric pressure is in the reverse direction with the cryo-deformation, the compensated quantity is derived by the sum of the vertical vector (2.98-1.32 = 1.66). After the first whole thermal cycles (from 1 December to 2 December), the realignment was taken out with the compensated quantity (1.66 mm) in the vertical direction to optimize the condition of the liquid nitrogen temperature. Since the cryo-contraction in the horizontal direction was symmetric, therefore, the compensated quantity was zero in the horizontal direction. In contrast, the vacuum-deformation seems different from each other; therefore, we did not

exert the compensation on the horizontal direction. Then the second thermal cycles was done to verify the correction of the compensated quantity. The right of the Fig. 7 shows that the differences of cryo-deformation (compensated) with respect to nominal zero in vertical direction is ±0.5mm. This resulted from plastic deformation [29][31] (0.15 mm in horizontal, 0.1 mm in vertical and 0.12 mm in the longitudinal direction, respectively shown in the Fig. 6) and the not fully released pressure of the vacuum.

The structural stability of the cryostat will be discussed as follows. First and foremost, suspension structure is the simplest but not the best structure for cryostat especially when the cryostat has stringent alignment requirements[5]. Furthermore, the facility for rare isotope beams of michigan state university has proven that the alignment of the bottom-up structure is more efficient than the suspend structure of cryostat[34-35]. Last but not least, since the bottom of the internal cooling mass has no direct contact with the external vacuum chamber of the suspend style cryostat, the cooling mass supported only by one force coming from the post in the vertical direction[36-37]. To sum up, we believe that the bottom-up structure is more stable than the suspend structure for cryostat.

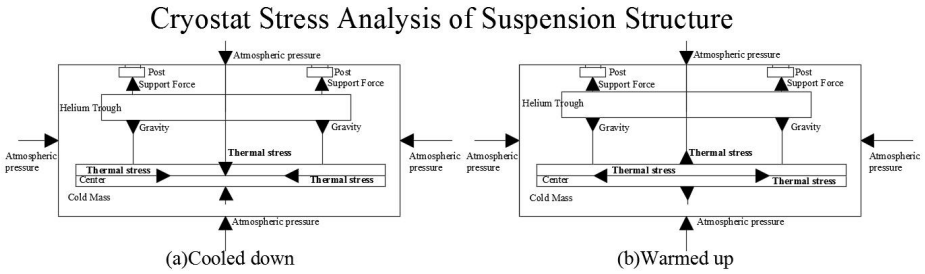

Fig. 8 Cryostat stress analysis of suspension structure

7 Conclusions

Cryostats are extremely complex systems, and their design optimization is strongly dependent on the accelerator application for which they are intended. We have demonstrated that the simulated vacuum and cryo-deformation shows a good agreement with the measured values. And the cryo-deformation is strongly linked with the vacuum negative pressure, temperature field and the structure of the cryostat. The above data provides information not only on the nature of the heat exchange phenomena and their effect on the structural stability of the internal components of the Cryostat, but also is a benefit to an optimization for the future Cryostats design. The analysis procedure will be helpful for the estimation of deformations in working conditions like mechanical and thermal loads. We will study the on-line continuous monitoring system in the future, which will further reveal low-temperature deformation mechanism of the cryostat. Finally, on June 5 to 7, 2017, the Chinese Accelerator Driven Subcritical System (CADS) Injector Ⅱ realized the pulse proton beam energy of 26.1 MeV, pulse current of 12.6 mA. And CADS achieved continuous wave proton beam energy of 25.0 MeV, continuous wave high power proton current of 150~200 uA for the first time in the world [32][33]. To sum up, the aligned accuracy fulfilled the requirements and the aligned results guaranteed the success of cw protons.

ACKNOWLEDGMENT

This work was financed by the National Natural Science Foundation of China (Study on the online monitoring of Cryomodule; (No.11605262)).

REFERENCE：

[1] Jijiu Zhao, Yin Zhao Sheng. Particle Accelerator Technology [M]. Beijing: Higher Education Press,2006:30-36(in Chinese).

[2] Zhihui Li, Peng Cheng, Huiping Geng, *et al*. Physics design of an accelerator for an accelerator-driven subcritical system [J]. PHYSICAL REVIEW SPECIAL TOPICS-ACCELERATORS AND BEAMS. 2013, 16, 080101-1:080101-23

[3] Shuhui Liu, Zhijun Wang, Huan Jia, *et al*. Physics design of the CIADS 25 MeV demo facility [J].Nuclear Instruments and Methods in Physics Research A.2017, 843:11-17

[4] Zhijui Wang, Chi Feng, Yuan He, *et al*. No interceptive transverse emittance measurements using BPM for Chinese ADS R&D Project [J].Nuclear Instruments and Methods in Physics Research A.2016, 816:171-175

[5] Weisend II, J. G. Cryostat Design [M].Springer; 1st ed. 2016 edition (August 13, 2016)
[6] G. Kautzmann, J-C. Gayde, F. Klumb, *et al*. HIE ISOLDE–GENERAL PRESENTATION OF MATHILDE [C]. The 13th International Workshop on Accelerator Alignment, 13-17 October 2014, IHEP, Beijing, P.R. China.
[7] Hiroshi Sakai, Kazuhiro Enami, Takaaki Furuya, *et al.* IMPROVEMENT OF THE POSITION MONITOR USING WHITE LIGHT INTERFEROMETER FOR MEASURING PRECISE MOVEMENT OF COMPACT ERL SUPERCONDUCTING CAVITIES IN Cryo module[C].The Proceedings of IPAC2014,Dresden,Germany,2014，TUPRI092:1787-1789.,
[8] A Bertolini. Vibration diagnostics instrumentation for ILC [J].Measurement Science & Technology -MEAS SCI TECHNOL, 2007, 18, 8: 2293-2298
[9] Hongyan Zhu, Lan Dong, Lingling Men, *et al.* Alignment of ADS beta cryostat with wire position monitors [J]. NUCLEAR SCIENCE AND TECHNIQUES, 2015, 26, 040401:1-4
[10] N. Eddy, B. Fellenz, P. Prieto, *et al*. A WIRE POSITION MONITOR SYSTEM FOR THE 1.3 GHZ TESLA-STYLE Cryostat AT THE FERMILAB NEW-MUON-LAB ACCELERATOR[C].The 15th International Conference on RF Superconductivity (SRF2011), Chicago, Illinois, USA, 25-29 Jul 2011, 2011, FERMILAB-CONF-11-382-AD.
[11] Remy BEUNARD, Alexis LEFEVRE, François LEGRUEL, SURVEY AND ALIGNMENT CONCEPT FOR THE SPIRAL2 ACCELERATOR (STATUS REPORT) [C].The 11th International Workshop on Accelerator Alignment, DESY, Hamburg, German, September 13-17, (2010)
[12] D. Passarelli, M. Parise, T. H. Nicol, *et al.* HIGH-VACUUM SIMULATIONS AND MEASUREMENTS ON THE SSR1 Cryo module BEAM-LINE[C].Proceedings of SRF2015, Whistler, BC, Canada, TUPB074:754-756
[13] Xiao Long Guo, Li Wang, Jin Wang, *et al.* Thermal and Mechanical Analysis on the Cold Mass Support Assembly of Test Cryostat for IMP ADS Injector-II [J]. Advances in Cryogenic Engineering, AIP Conf. Proc. 1573, 1341-1348 (2014); DOI: 10.1063/1.4860862
[14] Frank Marhauser and Kai Tian. Optimization of the Cryo module Cold-to-Warm Transitions and the VTA QA Test Configuration for CEBAF Upgrade Cavities with Regard to Critical HOMs above Cutoff [C].2009, JLAB-TN-09-61
[15] T Powers,T Allison,G Davis, *et al.* Upgrade to Cryo module Test Facility at Jefferson Lab[J].Accelerators, 2003
[16] Vittorio Parma. Cryostat Design [R].CERN Yellow Report (Accelerator Physics: Instrumentation and Detectors) CERN-2014-005, pp.353-399 DOI:10.5170/CERN-2014-005.353
[17] Li Wang, Sen Sun, Shuhua Wang, *et al*. design report of single test cryostat and control valve box in low temperature [R]
[18] J. R. Delayen, L.R. Doolittle, T. Hiatt, *et al.*AN R.F. INPUT COUPLER SYSTEM FOR THE CEBAF ENERGY UPGRADE Cryomodule [C]. Proceedings of the 1999 Particle Accelerator Conference, New York, 1999, 1462-1464
[19] Ruixiong Han, Lin Bian, Rui Ge, *et al*. Development of Vacuum Barrier in 2 K Transfer Lines for Accelerator-Driven Sub-Critical Reactor System [J].CHINESE JOURNAL OF VACUUM SCIENCE AND TECHNOLOGY, 2013, 33(11):1061-1064(In Chinese).
[20] Qingjin Xu, Ohuchi Norihito, Kiyosumi Tsuchiya, *et al*. Thermal simulation and analysis of the STF Cryostat[J].Chinese Physics C.2009, 33(3): 236-239
[21] Carlo Pagani and Paolo Pierini. Cryo module DESIGN, ASSEMBLY AND ALIGNMENT[C]. Proceedings of the 12th International Workshop on RF Superconductivity, Cornell University, Ithaca, New York, USA, SUP04:78-85
[22] A. Saini, V. Lebedev, N.Solyak, *et al.* ESTIMATION OF CRYOGENIC HEAT LOADS IN Cryostat DUE TO THERMAL RADIATION[C].Proceedings of IPAC2015, Richmond, VA, USA, WEPTY031:3338-3341
[23] Mubeezi, J., Finite Element Analysis (FEA) method, and its Application in Evaluating Stress-Strain Characteristics, Rensselaer at Hartford Engineering Seminar, 2004.
[24] T. S. Datta, Soumen Kar, Jacob Chacko, *et al.* Theoretical analysis for the transient behavior of radiative cooling of cavities in superconducting LINAC cryo module [J]. Heat Mass Transfer (2014) 50:827–833 DOI 10.1007/s00231-013-1281-1
[25] P. J. Barr, M.ASCE1,J. F. Stanton, *et al.* Effects of Temperature Variations on Precast, Prestressed Concrete Bridge Girders [J].JOURNAL OF BRIDGE ENGINEERING.2005, 10, 2:186-194 DOI: 10.1061/ (ASCE) 1084-0702(2005)10:2(186)
[26] Guicheng Du, Xin Ning, Yu Liu. Architectural Mechanics [M]. Dongbei University Publishing House, 2014
[27] Yu Qin Wan, Xiao Fei Niu, Yan Ning Han, *et al.* Cryostat design of ADS Injector Ⅱ [J]. Cryogenics and superconductivity, 2013,

41(12): 25-27
[28] Rui Ge, Ruixiong Han, Lin Bian, *et al.* Design of horizontal test cryostat for Spoke type SRF cavity [J]. CRYOGENICS, 2014, 3:7-10
[29] Jiandong Yuan, Yuan He, Bin Zhang. *et al*. Alignment of beam position monitors in cryomodule of CADS injector Ⅱ[J]. NUCL SCI TECH, (2017) 28: 75. https://doi.org/10.1007/s41365-017-0232-9
[30] A Bertolini, C Pagani, G Varisco. On line monitoring of the TTF Cryostat Cold Mass with Wire Position Monitors. 2000, Marzo, 17, INFN/TC-00/02
[31] N. V. Isaev, T. V. Grigorova, O. V. Mendiuk, *et al.* Plastic deformation mechanisms of ultrafine-grained copper in the temperature range of 4.2–300 K [J].LOW TEMPERATURE PHYSICS, 2016, 42, 9:825-835
[32] http://www.impcas.ac.cn/kyjz2017/201706/t20170622_4816973.html
[33] http://www.impcas.ac.cn/kyjz2017/201706/t20170622_4816980.html
[34] K. Saito, N. Bultman, E. Burkhardt, *et al.* SUPERCONDUCTING RF DEVELOPMENT FOR FRIB AT MSU[C].Proceedings of LINAC2014, Geneva, Switzerland, 2014, THIOA02
[35]T. Xu, H. Ao, B. Bird, *et al.*FRIB CRYOMODULE DESIGN AND PRODUCTION[C].Proceedings of LINAC2016, Geneva, Switzerland, 2016, WE2A02
[36]Jiandong Yuan.et al.Deformation Mechanism of the Cryostat in the CADS Injector Ⅱ[J]. Cryogenics 2018(89):113-118
[37]Jiandong Yuan.et al.Simulation Monitoring and Analysis for The Deformation of Cryomodule[J].Vacuum and Cryogenics 2018,24(3):182-187